Octave and Decade UWB Rectifiers Based on Non-Uniform Transmission Lines for Energy Harvesting

Octave and Decade UWB Rectifiers Based on Non-Uniform Transmission Lines for Energy Harvesting

John Kimionis, *Student Member, IEEE,* Ana Collado, *Member, IEEE,*
Manos M. Tentzeris, *Fellow, IEEE,* and Apostolos Georgiadis, *Senior Member, IEEE*

***Abstract*—Ambient RF energy harvesting is a potential energy source for low-power and battery-less wireless sensors, enabling a range of applications from monitoring to security as part of the Internet-of-Things scenario. One of the main challenges of ambient RF energy harvesting is the requirement of operation over a multitude of frequency bands of low ambient power densities resulting in a very wide aggregate operating bandwidth. In this paper, design examples of novel ultra-wide-band (UWB) energy harvesters are demonstrated with octave and decade bandwidths in the UHF and low microwave spectrum. The RF-dc conversion efficiency is maximized by tailoring the dimensions of a non-uniform transmission line used to provide broadband impedance matching. The design challenges in terms of impedance matching based on the Bode-Fano theoretical limit, losses and miniaturization are highlighted. Two prototypes are presented and their performance is evaluated. The octave band rectifier showed a measured RF-dc conversion efficiency of more than 60% over a frequency band of 470 MHz to 860 MHz at 10 dBm input power. The decade band rectifier fabricated on Kapton substrate using inkjet printing featured a higher than 33% efficiency over a frequency band from 250 MHz to 3 GHz at 10 dBm input power.**

***Index Terms*— Rectifier, RF energy harvesting, wireless power transfer, UWB, inkjet printing, flexible electronics, non-uniform transmission line, Internet-of-Things.**

I. Introduction

HARVESTING ambient RF energy to power wireless sensors and transmitters is receiving significant attention nowadays, due to an increasing interest in compact, low power, and even battery-less sensors enabling the concept of the Internet-of-Things which encompasses a growing number of applications from smart metering and monitoring in general to security, health and well-being [1]. There is a significant amount of publications in the recent literature regarding the performance analysis of rectennas and rectifiers especially due to the recent interest in energy harvesting and wireless powering for IoT applications [1][2]. There are several important earlier works on diode detectors [3], and theoretical estimation of the efficiency of diode rectifiers [4], as well as more recent publications such as [5][6][7] addressing the performance as RF-dc power conversion circuits in low power far-field wireless power transfer or RFID applications.

There are several examples in the recent literature demonstrating the ability to power sensors using the energy available from various broadcast transmitters including, FM, TV, cellular or Wi-Fi systems [8][9]. One characteristic of such transmissions is the time-/space-varying variable nature of the available power density, due to a variety of reasons such as complex propagation settings as well as varying demand and broadcasting schedules. As a result, one has to be able to harvest RF energy within a large aggregate spectrum to guarantee the harvesting of sufficiently high aggregate power for practical applications. In rectenna and rectifier design, it is a challenge to maximize the RF-dc conversion efficiency over a wide aggregate bandwidth including multiple narrower frequency bands or an ultra-wide single frequency band. This is important in order to maximize the total harvested RF energy from broadcast transmissions at different frequencies. Recent publications of dual band, triple or quadruple band rectifier circuits include [10][11][12] and 3-dimensional topologies have been recently explored for harvesting RF power from multiple directions [13] without compromising communication [14].

In order to address the wideband harvesting requirement, a novel ultra-wideband rectifier is introduced in this paper. The equivalent RC circuit of different rectifiers for a variety of different input power excitation and output load values is extracted and the theoretical minimum reflection coefficient over a desired frequency band based on the Bode-Fano theory [15] is investigated. Based on this study a rectifier circuit topology is selected and its impedance matching circuit is designed in a broadband way. A non-uniform microstrip transmission line in series with an inductor is selected to implement the matching network and harmonic balance optimization is used to maximize the RF-dc rectifier efficiency. Preliminary results of this work are presented in [16], where a rectifier circuit with an octave bandwidth was designed. In this work, in addition to further design and

The work of A. Georgiadis and A. Collado was supported by EU H2020 Marie Sklodowska-Curie Grant Agreement 661621 and by COST Action IC1301 Wireless Power Transmission for Sustainable Electronics. The work of J. Kimionis and M.M. Tentzeris was supported by the National Science Foundation (NSF) and the Defense Threat Reduction Agency (DTRA).

A. Georgiadis and A. Collado are with Heriot-Watt University, Edinburgh, UK (e-mail: apostolos.georgiadis@ieee.org, ana.collado@ieee.org).

J. Kimionis and M.M. Tentzeris are with Georgia Institute of Technology, Atlanta, GA 30332, USA, (e-mail: ikimionis@gatech.edu, etentze@ece.gatech.edu).

optimization details of the aforementioned rectifier, a second rectifier design is presented covering more than a decade bandwidth. Additionally, the proposed rectifier is simultaneously optimized in order to minimize its size and a flexible substrate and inkjet printing fabrication are used to demonstrate a proof-of-concept conformal implementation using low cost additive manufacturing. Prototypes of the two rectifiers have been fabricated and tested showing good agreement with simulations. The octave band rectifier has an RF-dc conversion efficiency varying within [5.5%, 13.5%] from 475 MHz to 975 MHz for -20 dBm input available power, and more than 60% efficiency from 470 MHz to 860 MHz when the input power is 10 dBm. The decade rectifier has an efficiency within [4.5%, 7%] for -10 dBm input power and more than 33% for 10 dBm input power between 250 MHz and 3 GHz, for a load of 1.3 KΩ.

The paper is structured as follows: In Section II, the equivalent circuit of different generic rectifier architectures is derived and the minimum reflection coefficient is evaluated based on the Bode-Fano theory. In Section III, the design and optimization procedure of the non-uniform transmission line matching network are described and two rectifiers with an octave and decade bandwidth respectively are presented. Finally, Section IV presents a summary of this work's results.

II. Bode-Fano Reflection Coefficient Limit For UWB Rectifier Impedance Matching

According to the theory originally developed by Bode and extended by Fano [15], the minimum reflection coefficient magnitude $|\Gamma_m|$ which can be obtained by a lossless matching network connected to a load impedance consisting of a shunt resistor R_e and a shunt capacitor C_e over a bandwidth B is limited by

$$|\Gamma_m| \geq e^{-\frac{1}{2BR_eC_e}} \qquad (1)$$

where a constant reflection coefficient $|\Gamma_m|$ over the bandwidth B and unity reflection coefficient over the rest of the spectrum is assumed.

The input impedance of a series diode rectifier, or charge pump (voltage N-tupler) rectifier, such as the ones shown in Fig. 1, for a given input power and output load resistance is equivalent to the input impedance of a shunt RC circuit. This can be easily verified using a commercial nonlinear circuit simulator such as harmonic balance.

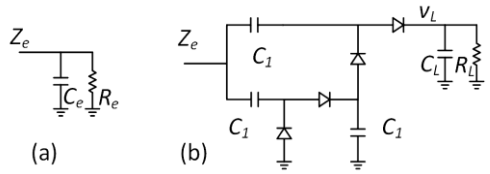

Fig. 1. Rectifier input impedance, a) equivalent circuit, b) charge-pump rectifier with four diodes.

In a first example [16], the equivalent circuits of different rectifier circuits of a series diode topology and of different charge pump rectifiers with two, four and six diodes were evaluated. The rectifier circuit capacitors C_1 = 100 pF and C_L = 10 nF were set to sufficiently large values to represent an effective short circuit at the frequency band 0.4 GHz – 1 GHz under consideration. It was shown that the equivalent capacitance C_e was proportional to the number of diodes and approximately independent of the output load resistance and of the input power values [16]. The equivalent diode resistance R_e was approximately inversely proportional to the number of diodes and depended both on the input power level and the output load resistance [16]. Due to this fact the product of R_e and C_e, depends on the number of diodes in the rectifier circuit and consequently the minimum reflection coefficient (1) depends on the input power, the output load resistance as well as on the number of diodes.

The minimum reflection coefficient obtained using (1) for frequency band of 0.4 GHz – 1.0 GHz is plotted in Fig. 2. One can see that it is easier to minimize the reflection coefficient at higher input power levels and at lower load resistance values. Furthermore, the series diode rectifier appears to be more difficult to match than rectifier charge pump circuits with more diodes. Based on the result of Fig. 2 a rectifier with four diodes was selected in order to design an energy harvester covering the band from 0.4 GHz to 1.0 GHz.

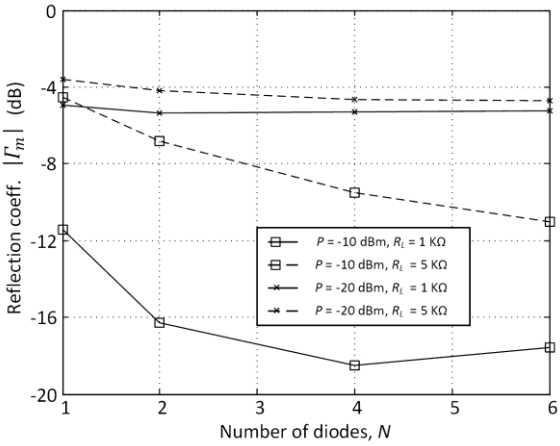

Fig. 2. Theoretical minimum reflection coefficient in the frequency band of 0.4 GHz – 1.0 GHz versus the number of diodes for different input power and output load resistance values.

The equivalent input resistance and capacitance of various rectifier circuits with N = 1,2,4 and 6 diodes and load resistance R_L = 1KΩ are plotted versus the available input RF power P in Fig. 3. One can see that the nonlinear nature of the capacitance becomes evident for power levels near 0 dBm and above. In addition, the strong dependence of the input resistance on the input power is evident.

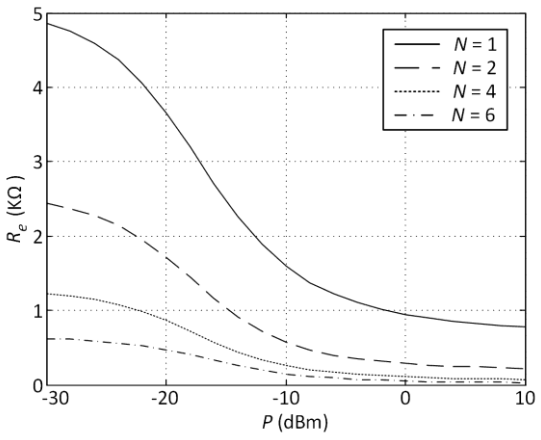

(a)

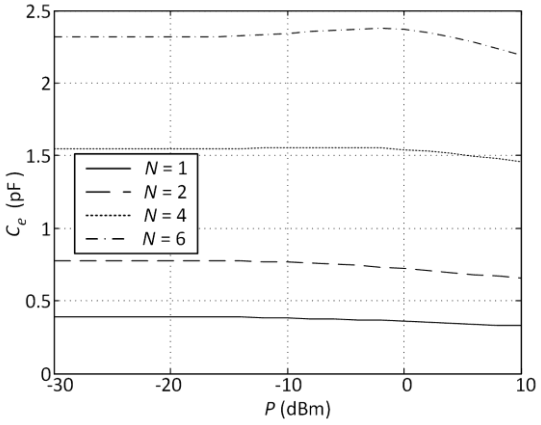

(b)

Fig. 3. Rectifier equivalent input impedance versus input power a) resistance and b) capacitance for rectifiers with a different number of diodes *N*. The output load resistance is 1KΩ.

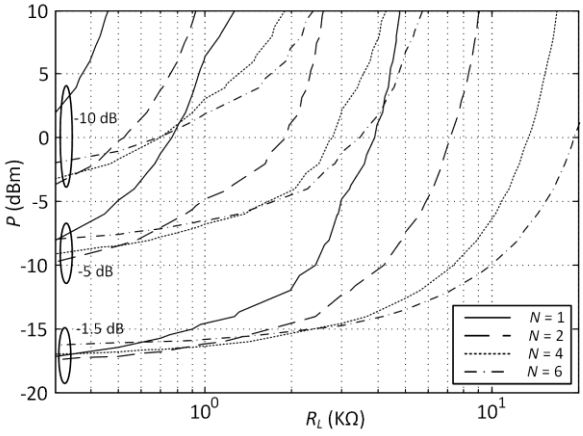

Fig. 4. Rectifier minimum reflection coefficient (dB) contours versus input power and load resistance for UWB rectifier circuits with a different number of diodes N.

In a second more broadband example, a rectifier with a more-than-decade bandwidth from approximately 0.25 GHz to 3 GHz was considered. Using the obtained equivalent resistance and capacitance values and (1), contours of theoretical minimum reflection coefficient were computed for different load resistance input power and number of rectifier diodes, as shown in Fig. 4. Once again it is verified that a lower reflection coefficient can be theoretically obtained for higher input power levels and smaller load values. Furthermore, the series diode rectifier is more difficult to match, while there is little improvement going from 4 to 6 diode rectifiers. In order to maintain a minimum circuit complexity a 2-diode rectifier was selected for the decade band design.

III. Ultra-broadband Rectifier Design

A non-uniform transmission line in series with a lumped inductor L_1 was chosen to implement the impedance matching network for the introduced ultra-broadband rectifier. Non-uniform transmission lines have been traditionally used to provide broadband matching to real loads as shown by the selected examples of [17][18]. In addition, they can be used to provide dispersion compensation in optical communication links [19]. In this work a series inductor is first used to provide narrowband matching and cancel the capacitive imaginary part of the rectifier impedance around a certain frequency within the band under consideration. Then a non-uniform transmission line transforms the low-imaginary-part complex impedance to the desired 50 Ω source impedance. The matching network is shown in Fig. 5. A microstrip line consisting of trapezoidal sections was used to implement the non-uniform transmission line. Coplanar waveguide or grounded coplanar waveguide lines can also be used, however microstrip line was chosen for the proof-of-concept prototypes in order in order to minimize fabrication time and minimize the need for plated through via holes or bridges.

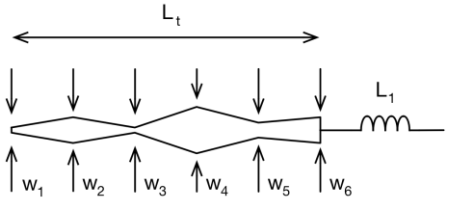

Fig. 5. Rectifier impedance matching network consisting of a series inductor and a non-uniform transmission line.

The rectifier RF-dc conversion efficiency is defined as

$$\eta = \frac{P_{dc}}{P} \qquad (2)$$

where $P_{dc} = V_L^2/R_L$ and V_L is the output dc voltage and R_L the output load resistance. P is the available RF power at the input of the rectifier. In this effort, η is maximized over the broadest desired frequency band for a given input power P using harmonic balance optimization while optimization parameters include the non-uniform transmission line, the inductor L_1 and the load R_L.

A. Octave Bandwidth Rectifier

As a proof-of-concept, an octave bandwidth rectifier for the 400 MHz to 1 GHz band was designed using a four diode charge pump rectifier and a non-uniform transmission line of

TABLE I
RECTIFIER OPTIMIZATION PARAMETERS,
P = -20 DBM

Param.	Value	Param.	Value
w_1	2.65 mm	w_6	6 mm
w_2	2.72 mm	L_t	174.5 mm
w_3	3.62 mm	L_1	20 nH
w_4	6 mm	R_L	12.2 KΩ
w_5	1 mm		

length L_t consisting of five trapezoidal sections of equal length as shown in Fig. 5. The Skyworks SMS7630 diode was used, and the package parasitics were taken into account for the design process. A parasitic inductance value of $L_p = 0.6$ nH and a parasitic capacitance value of $C_p = 0.25$ pF provided by the manufacturer were added in the design schematic (Fig. 6-top). The selected substrate was Arlon A25N with dielectric permittivity 3.38, loss tangent 0.0025 and 20 mil thickness. The minimum line width in the optimization process was set to 0.3 mm in order to facilitate fabrication with a circuit mill. The full rectifier schematic is shown in Fig. 6-middle, with the matching network including the 5-section non-uniform transmission line and the series lumped inductor L_1. Coilcraft inductors were used for the designs, with all surface mount device (SMD) package parasitics accounted in the simulations and optimization. The circuit parameters were optimized with Keysight Advanced System (ADS) in Harmonic Balance mode using gradient optimization, with a goal of maximizing the efficiency value η. Note that this does not necessarily optimize the return loss S_{11}, since the main goal of the rectifier is to deliver as much power to the load R_L as possible, rather than minimize reflections at the RF input port. The initial value of the total line length L_t was arbitrarily set to 15 cm and was allowed to optimize. This value corresponds to an electrical length of approximately 185 degrees at 632 MHz which is the geometric mean between the operating band edges of 0.4 GHz and 1GHz. For this octave bandwidth rectifier, all transmission line sections were equal, with length $L_t/5$.

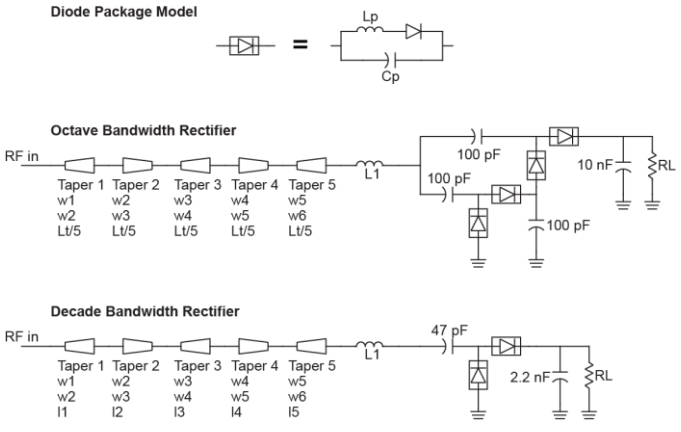

Fig. 6. Top: SMS730 diode parasitic model. Middle: Optimization schematic for octave bandwidth rectifier with non-uniform transmission line. Bottom: Optimization schematic for decade bandwidth rectifier with non-uniform transmission line.

Table I shows the result of the optimization process including the final dimensions of the transmission line sections, the inductor value and the optimum load at -20 dBm input power. The fabricated prototype, shown in Fig. 7, was measured with a lab setup to characterize the input S-parameters and conversion efficiency for different power levels and load values. The input S-parameter measurements were obtained using a network analyzer in frequency sweep mode and varying port power. The RF-dc conversion efficiency measurements were obtained using a signal generator to provide a continuous wave (CW) signal at a given power level and the dc output voltage was measured using a digital multimeter (DMM). The output load was set using a trimmer resistor and measured using the DMM. The RF power level at the input of the rectifier was measured using a spectrum analyzer and cable losses were characterized using a network analyzer/cable tester. The dc output voltage value was converted to output power value using the measured load resistance and the efficiency was calculated as the ratio of Eq. (2).

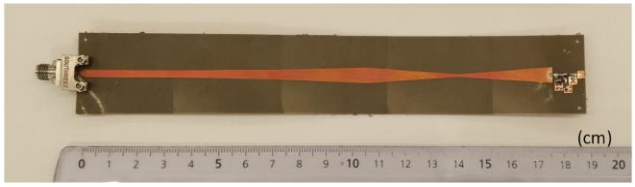

Fig. 7. Octave bandwidth rectifier prototype.

The rectifier's input S-parameters are shown in Fig. 8-top, where a good agreement between simulation and measurements is obtained. In accordance with Section II, one can see that as the input power increases and the rectifier output load resistance decreases, impedance matching is improved. For power levels of 0 dBm and 10 dBm and respective load values of 5.5 KΩ and 3 KΩ, the return loss is better than -10 dB within the whole band of interest, and the curves have been omitted for clarity. As aforementioned, the optimization goal for the rectifier was the maximum efficiency and not minimized return loss. Thus, the curves of Fig. 8-top can be used for *relative* comparison of the rectifier's behavior under different input power levels and output load values. Fig. 8-bottom shows the input reflection coefficient in Smith Chart form for an input power level of -10 dBm and a load value of $R_L = 7$ KΩ.

The rectifier RF-dc conversion efficiency was evaluated for different input power levels and it is presented in Fig. 9-top. The optimum load was also investigated experimentally and the plots of Fig. 9-top include the prototypes' load values chosen as close as possible to the optimum value based on the available resistors for the measurements. Simulation results are compared for the same load value at each given input power level showing a very good agreement. The measured efficiency varies from approximately 5.5% at 475 MHz to 13.5% at 975 MHz for an input power level of -20 dBm,

exceeding an octave bandwidth of operation. In addition, the efficiency remains above 60% at 10 dBm input power over a bandwidth of 390 MHz, from 470 MHz to 860 MHz. It is noted that the optimum load leading to maximum efficiency is reduced with increasing input RF power. This has been studied in detail in [20] and is consistent within the simulation and measurement results of this work. In Fig. 9-bottom, the simulated RF-dc conversion efficiency is also shown for varying input power levels from -20 dBm to 10 dBm, for a *fixed* load value of $R_L = 12$ KΩ, which corresponds to the optimal load value for $P = -20$ dBm.

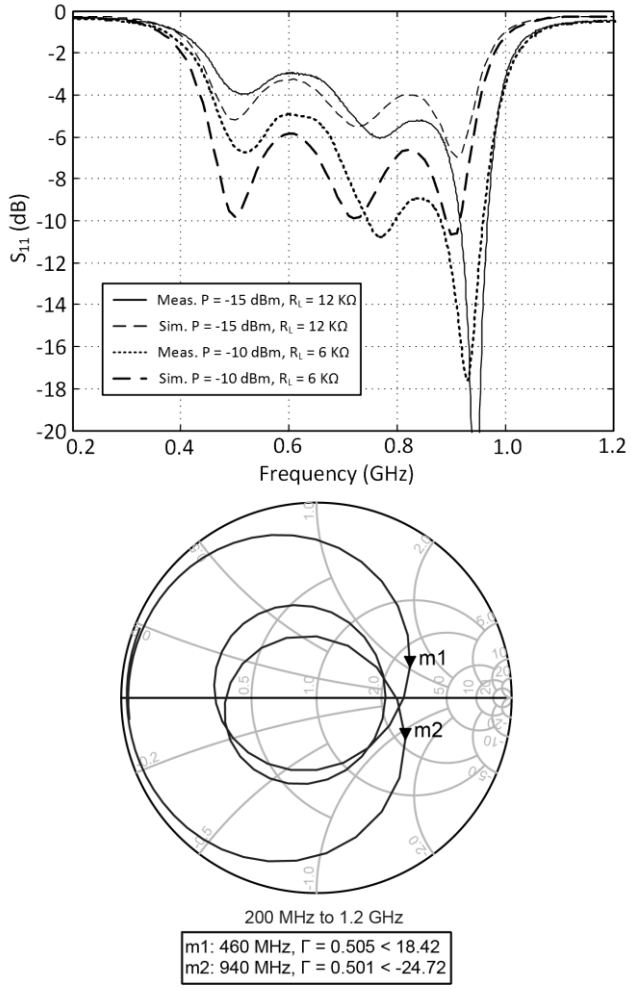

Fig. 8. Input S-parameters of the octave band rectifier. Top: Return Loss. Bottom: S_{11} Smith Chart for input power P = -10 dBm and $R_L = 7$ KΩ.

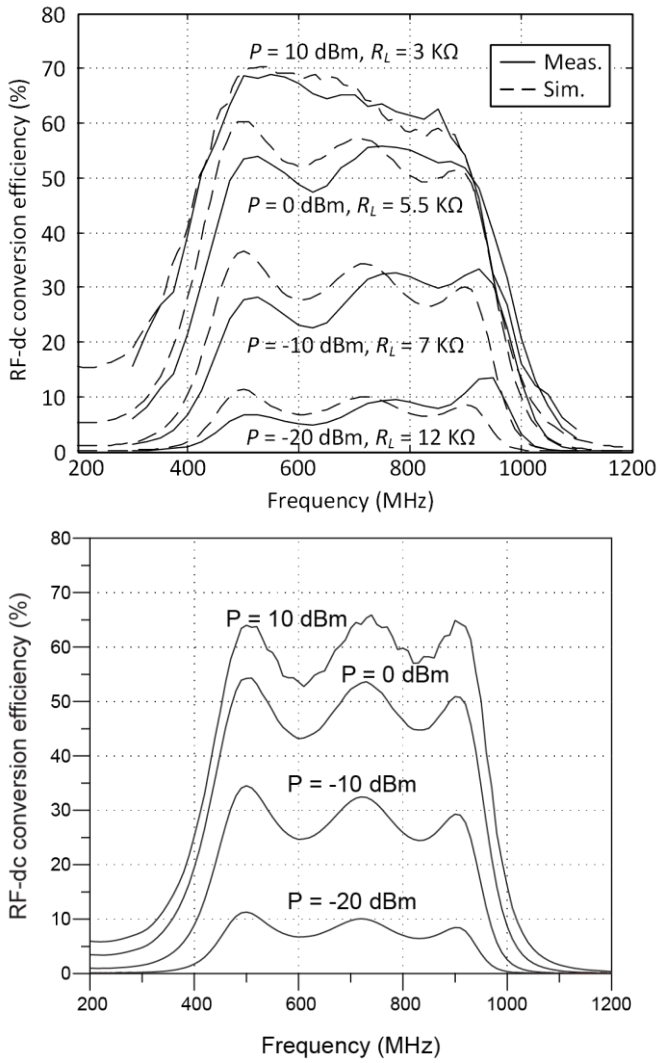

Fig. 9. Octave bandwidth rectifier RF-dc conversion efficiency. Top: Measurement and simulation for varying power levels and optimal load per power level. Bottom: Simulation for varying power levels and fixed load value of 12 KΩ.

B. Decade bandwidth rectifier on flexible substrate

The decade bandwidth rectifier was designed to achieve its optimal operation at 3 GHz with an inkjet printing implementation on a flexible polyimide (Kapton) substrate with dielectric constant ε_r = 3.4, loss tangent tanδ = 0.0025, and 5 mil thickness. A two-diode rectifier is designed to drive a load of 1.3 KΩ with an input power level of as low as -10 dBm. The same diode was used (Skyworks SMS7630) for the decade bandwidth rectifier and ADS was used in Harmonic Balance mode to optimize the circuit of Fig. 6-bottom with a gradient optimization algorithm. The optimization goal is the maximization of the RF-dc conversion efficiency between 250 MHz and 3 GHz, without any target goal for the return loss.

A non-uniform transmission line is designed and optimized for the UWB rectifier for decade-broadband matching. The transmission line length is kept significantly low compared to the octave rectifier to minimize the losses of inkjet-printed traces that feature lower conductivity levels (5×10^6 S/m) compared to the copper cladding of standard PCBs (5.8×10^7 S/m). The microstrip line mainly targets the higher frequencies of the band, where diodes typically show low efficiency performance. The effect of matching with the non-uniform transmission line can be clearly seen in Fig. 10, where the simulated RF-dc conversion efficiency of the two-diode rectifier driving a 1.3 KΩ load with and without UWB matching are shown for -10 dBm input power. `No matching' refers to the case of directly feeding the RF power to the voltage doubler without the lumped inductor and non-uniform transmission line. It is apparent that with the UWB matching network, consisting of the inductor L1 and non-uniform transmission line, the average efficiency across the band is increased, with a peak around 1500 MHz that is the center of the band. Notice that the peak has a value of 8%, while an average efficiency of 7% spans a very wide frequency region of 3 GHz. This is in contrast with conventional harvesters that are optimized for a specific power and frequency point and achieve higher efficiency values, albeit around a very tuned frequency point. This has a result of a very sharp efficiency decay when the excitation signal is slightly detuned from the precisely-tuned operating point of the harvester. This work's decade bandwidth harvester features a steady efficiency value across a very wide band, which can facilitate the design of additional dc-dc converters, supercapacitor charging circuits, and power management units at the output of the harvester.

TABLE II
UWB RECTIFIER OPTIMIZATION PARAMETERS, P = -10 DBM

Param.	Value	Param.	Value
w_1	1.76 mm	l_2	5.95 mm
w_2	0.24 mm	l_3	4.79 mm
w_3	0.11 mm	l_4	2.12 mm
w_4	0.23 mm	l_5	0.1 mm
w_5	3.43 mm	L_t	14.22 mm
w_6	1 mm	L_1	3.6 nH
l_1	1.25 mm	R_L	1.3 KΩ

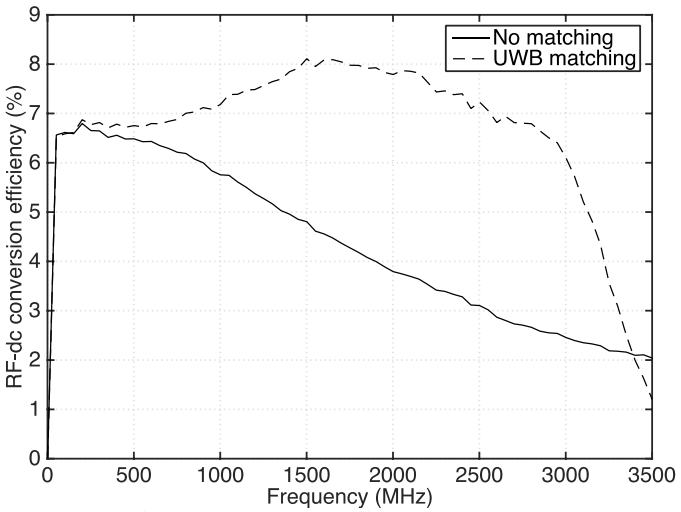

Fig. 10. Rectifier RF-dc conversion efficiency without and with UWB matching (RF input power -10 dBm, load value 1.3 KΩ).

Due to the nature of inkjet printing, where high resolution of printed features can be achieved, the non-uniform transmission line for the UWB harvester was not constrained to a minimum width of 0.3 mm, as in the case of the octave band harvester fabricated on a rigid substrate. As shown in Table II, the smallest required width of the UWB matching line is 100 μm, which can be precisely achieved with inkjet printing. Moreover, for the UWB transmission line, the tapered sections do not all feature the same length, in order to double the degrees of freedom for the design and minimize any potential losses. The line sections' width (w_i) and length (l_i) values as well as the matching inductor value can be seen in Table II. The total line length is less than 1.5 cm, keeping the total system (harvester circuit and line) area less than 2 cm^2.

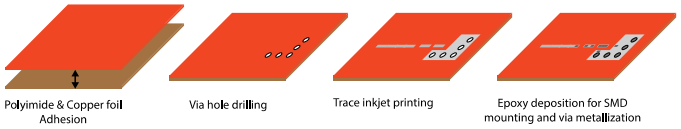

Fig. 11. Printed board fabrication process.

The fabrication of the decade UWB harvester prototype board, before placing the SMD components (0603 size), involves 4 steps, shown in Fig. 11:

1) Substrate preparation by attaching an adhesive copper foil (copper tape) under the polyimide film to form the microstrip ground plane.

2) Drilling to form the holes of the vias required for ground connections.

3) Inkjet printing of traces with a conductive silver nanoparticle ink.

4) Conductive epoxy deposition for via metallization and SMD component attachment.

The holes on the substrate are drilled right after attaching the copper tape to the polyimide film and before printing the silver to avoid any cracks on the printed traces (Fig. 12-left). Apart from the 0.8 mm-diameter holes drilled for vias, two 2 mm-diameter holes are also drilled to mount an SMA end-launch connector.

A Dimatix DMP-2800 inkjet printer is used to deposit droplets of silver nanoparticle (SNP) ink on the substrate to

form the traces of the non-uniform line and the circuit component pads. Five layers of silver nanoparticle ink are deposited with 20 μm drop spacing on a 60º C-hot platen and an inter-layer printing delay of at least 300 seconds, to guarantee enough time for SNP ink solvent evaporation which will minimize ink spreading. This is crucial especially for the thinnest parts of the line, where the line width (100 μm) consists of only 4-5 SNP drops. The board is placed in a temperature-controlled oven at 180º C for at least 60 minutes to ensure full SNP sintering that will maximize conductivity. The fully-cured board can be seen in Fig. 12-right, with the SNP ink printed directly on top of the vias.

It is interesting to note that printing directly on the drilled substrate creates SNP walls in the holes that electrically connect the printed silver traces with the copper ground plane. The resistance between the top silver trace and the copper ground plane is less than 4 Ω. However, a low resistivity silver epoxy (0.0007 Ω•cm) is used for via metallization to improve operation at high frequencies as well as for SMD component mounting. The epoxy consists of two parts that need to be mixed together to start the curing process. Due to the small SMD sizes (order of millimeters) a controlled dispensing method is needed to precisely deposit the conductive adhesive on the silver traces. A novel method is tested, inspired by solder paste deposition tools, that involves a solder paste deposition pump that applies air pressure to a syringe with a piston for micro-dispensing of paste on circuit traces. Because conductive epoxies are typically two-part materials that start curing immediately after mixing (even at room temperatures), the epoxy chosen has a long working time (4 hr), which is enough for mixing, transferring to a 10 cc syringe tube, and connecting to the deposition pump for dispensing, before starting hardening up to a non-working viscosity level. The pump pressure is set to at least 0.2 MPa to dispense the mixed epoxy with a 26-gauge tip. The via holes are filled with epoxy which accumulates on the via walls, creating shorts between the top printed traces and the copper ground plane. Drops of epoxy are also dispensed on the printed traces at the positions where the SMD pads are going to be attached. After placing the components, the board is oven-heated at a moderate temperature of 65º C for at least 60 minutes. A microscope photograph of the attached SMD components and metallized vias is shown in Fig. 13. The fully-assembled harvester board (2.5x0.75 cm) with the attached end-launch connector is shown in Fig. 14.

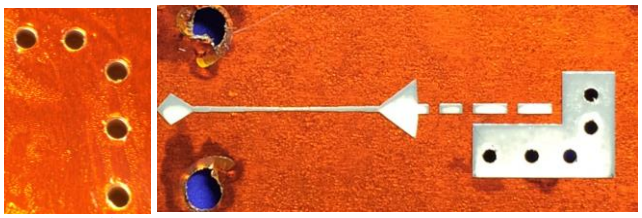

Fig. 12. Left: Drilled via holes on polyimide and copper tape substrate. Right: Inkjet-printed board; feeding section, non-uniform transmission line, and SMD components pads.

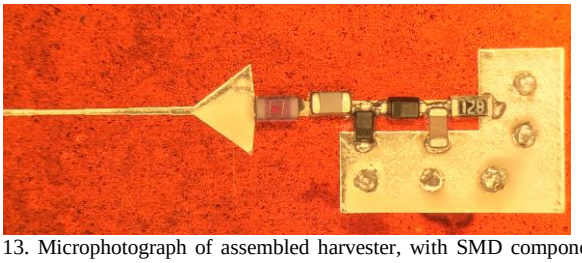

Fig. 13. Microphotograph of assembled harvester, with SMD components and epoxy-metallized vias.

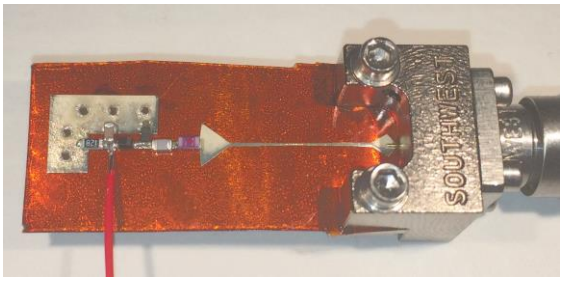

Fig. 14. Flexible UWB harvester prototype with end-launch SMA connector and V_{out} testing output.

The simulated input S-parameters along with the VNA-measured S-parameters of the UWB harvester prototype are shown in Fig. 15-top and a Smith Chart of the input reflection coefficient is shown in Fig. 15-bottom for an input power of 0 dBm. A signal generator and a digital multimeter (DMM) have been used to measure the harvester output voltage level for various input power levels and frequency points. The 2-D function $V_{\text{out}} = f(F, P)$ contours are shown in Fig. 16 for the simulated circuit and measured prototype. The x-axis is the frequency variation and the y-axis is the input power variation. The tone of grey denotes the level (output voltage) of each contour, according to the color bar on the right, i.e. the output voltage increases as the input power increases for a given frequency, and the output voltage remains stable across frequency variations for any given input power level. It can be seen that the output power level for a given input power shows very little variation in the whole band of interest between 250 MHz to 3 GHz. In Fig. 17, the efficiency across the frequency band is plotted for three input power levels, -10, 0, and 10 dBm. The measured efficiency increases from 6% on average for -10 dBm input power to 37% on average for 10 dBm input power. The efficiency shows small variations within the band between 250 MHz and 3 GHz, between [4.5%, 7%] for an input power level of -10 dBm, [18%, 25%] for 0 dBm, and [32.5%, 40%] for 10 dBm input power. Even though the efficiency is increased for high power levels, there are applications where high-level RF power is available e.g. from handheld devices such as radios. The work in [21] has successfully demonstrated the exploitation of ambient nearby sources for powering up wearable devices. In our work, we leverage the potential of such high power availability, by enabling an ultra-wideband operation of flexible printed harvesters that can be integrated with wearables and exploit power from handheld radios, cellphones, desktop Wi-Fi access points, etc.

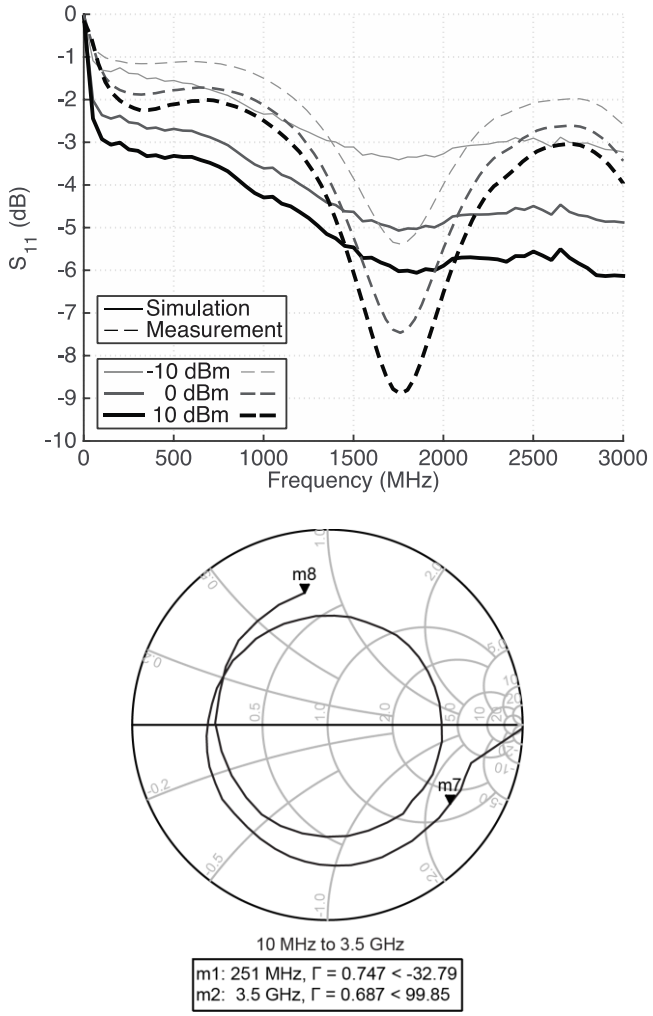

Fig. 15. Input S-parameters of the decade band rectifier (R_L = 1.3 KΩ). Top: Return Loss. Bottom: S_{11} Smith Chart for input power P = 0 dBm and R_L = 1.3 KΩ.

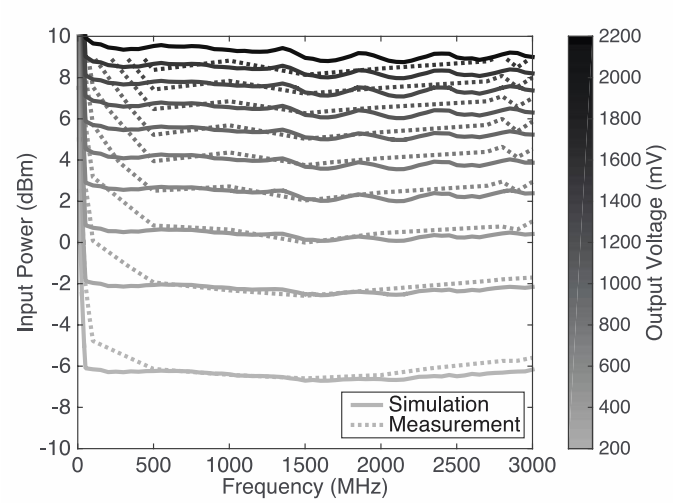

Fig. 16. Contours of simulated and measured rectifier dc output voltage for varying input power level and frequency values (R_L = 1.3 KΩ).

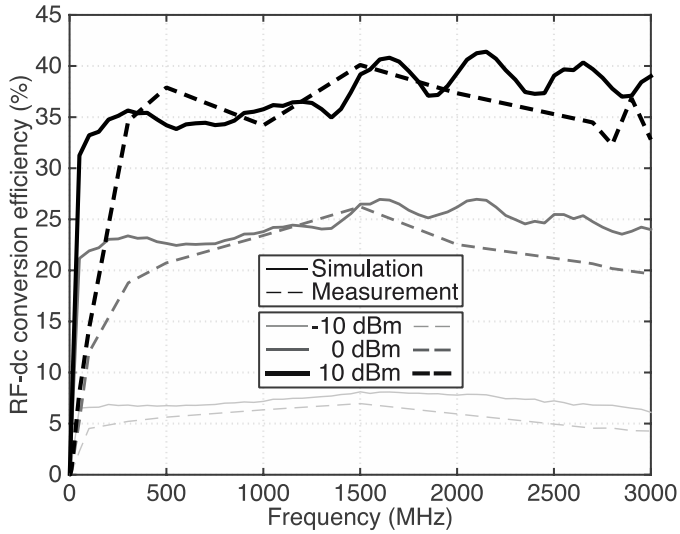

Fig. 17. Simulated and measured efficiency for UWB harvester (R_L = 1.3 KΩ).

In comparison with existing UWB rectifiers in the literature, both the octave and decade bandwidth rectifiers presented in this work achieve RF-dc conversion efficiency values that are significantly flatter (less than 10% efficiency fluctuation) versus frequency variations for any given power level. As an example, the octave bandwidth rectifier presented in [22] achieves an RF-dc conversion efficiency that greatly varies from 20% to 80% for frequencies between 650 MHz and 1.05 GHz at a high input power level of +20 dBm and only achieves a flat efficiency value for varying frequency at its highest operating input power of 40 dBm.

IV. Conclusion

This paper has presented the design of UWB rectifiers that utilize non-uniform transmission lines for broadband matching. Two prototype harvesters have been implemented and characterized to prove the feasibility of ultra-wideband matching with non-uniform transmission lines. The first, which features a 4-diode charge pump and is implemented on a rigid substrate, achieved a measure RF-dc conversion efficiency of more than 60% for an octave frequency band of 470 MHz to 860 MHz at 10 dBm input power. The second, which features a 2-diode charge pump and is inkjet-printed on a flexible substrate targeting conformal applications, achieved an efficiency of more than 33% for an ultra-wide frequency band between 250 MHz and 3 GHz.

References

[1] S. Kim, R. Vyas, J. Bito, K. Niotaki, A. Collado, A. Georgiadis, M.M. Tentzeris, "Ambient RF Energy-Harvesting Technologies for Self-Sustainable Standalone Wireless Sensor Platforms," *Proc. of the IEEE*, vol.102, no.11, pp.1649-1666, Nov. 2014.

[2] J.A. Hagerty, F.B. Helmbrecht, W.H. McCalpin, R. Zane, Z.B. Popovic, "Recycling ambient microwave energy with broad-band rectenna arrays," IEEE Trans on Microw Theory and Techniques vol. 52, no. 3, pp. 1014-1024, Mar. 2004.

[3] R. G. Harrison, "Full nonlinear analysis of detector circuits using Ritz-Galérkin theory," in Proc. IEEE MTT-S Int. Microwave Symp. Dig., Albuquerque, NM, 1992, pp. 267–270.

[4] T.-W. Yoo, K. Chang, "Theoretical and experimental development of 10 and 35 GHz rectennas," IEEE Transactions on Microwave Theory and Techniques, vol. 40, no. 6, pp. 1259-1266, Jun 1992.
[5] J.A.G. Akkermans, M.C. van Beurden, G.J.N. Doodeman, H.J. Visser, "Analytical models for low-power rectenna design," IEEE Antennas and Wireless Propagation Letters, vol. 4, pp. 187-190, 2005.
[6] G. De Vita, G. Iannaccone, "Design criteria for the RF section of UHF and microwave passive RFID transponders," IEEE Trans on Microw Theory and Techniques, vol. 53, no. 9, pp. 2978-2990, Sep. 2005.
[7] S. D. Assimonis, S. N. Daskalakis and A. Bletsas, "Sensitive and Efficient RF Harvesting Supply for Batteryless Backscatter Sensor Networks," in *IEEE Transactions on Microwave Theory and Techniques*, vol. 64, no. 4, pp. 1327-1338, April 2016.
[8] R.J. Vyas, B.B. Cook, Y. Kawahara, M.M. Tentzeris, "E-WEHP: A Batteryless Embedded Sensor-Platform Wirelessly Powered from Ambient Digital-TV Signals," *IEEE Trans. Microw. Theory Techn.*, vol.61, no.6, pp.2491-2505, June 2013.
[9] A. N. Parks, A.P. Sample, Y. Zhao, J.R. Smith, "A wireless sensing platform utilizing ambient RF energy," in 2013 IEEE Topical Conf. on Biomedical Wireless Techn, Networks, and Sensing Systems (BioWireleSS), pp.154-156, 20-23 Jan. 2013.
[10] A. Collado and A. Georgiadis, "Conformal Hybrid Solar and Electromagnetic (EM) Energy Harvesting Rectenna," in IEEE Transactions on Circuits and Systems I: Regular Papers, vol. 60, no. 8, pp. 2225-2234, Aug. 2013.
[11] B. L. Pham and A. V. Pham, "Triple bands antenna and high efficiency rectifier design for RF energy harvesting at 900, 1900 and 2400 MHz," Microwave Symposium Digest (IMS), 2013 IEEE MTT-S International, Seattle, WA, 2013, pp. 1-3.
[12] D. Masotti, A. Costanzo, M. D. Prete and V. Rizzoli, "Genetic-based design of a tetra-band high-efficiency radio-frequency energy harvesting system," in IET Microwaves, Antennas & Propagation, vol. 7, no. 15, pp. 1254-1263, December 10 2013.
[13] J. Kimionis, M. Isakov, B. S. Koh, A. Georgiadis and M. M. Tentzeris, "3D-Printed Origami Packaging with Inkjet-Printed Antennas for RF Harvesting Sensors," in *IEEE Transactions on Microwave Theory and Techniques*, vol. 63, no. 12, pp. 4521-4532, Dec. 2015.
[14] J. Kimionis and M. M. Tentzeris, "RF tag front-end design for uncompromised communication and harvesting," *2014 IEEE RFID Technology and Applications Conference (RFID-TA)*, Tampere, Finland, 2014, pp. 109-114.
[15] R.M. Fano, "Theoretical limitations on the broadband matching of arbitrary impedances," Research Laboratory of Electronics, Massachusetts Institute of Technology, MA, Tech. Rep. No. 41, Jan. 2, 1948.
[16] F. Bolos, D. Belo, A. Georgiadis, " A UHF Rectifier with One Octave Bandwidth Based On a Non-Uniform Transmission Line," *in 2016 IEEE MTT-S Intl. Microw. Symposium (IMS)*, 22-27 May 2016.
[17] H. Oraizi, "Design of impedance transformers by the method of least squares," in *IEEE Trans. Microw. Theory Techn*, vol.44, no.3, pp.389-399, Mar. 1996.
[18] Y.-W. Hsu, E.F. Kuester, "Direct Synthesis of Passband Impedance Matching with Nonuniform Transmission Lines," *IEEE Trans. Microw. Theory Techn*, vol.58, no.4, pp.1012-1021, April 2010.
[19] L. Ranzani, P. Boffi, R. Siano, S. Rondineau, Z. Popovic, M. Martinelli, "Microwave-Domain Analog Predistortion Based on Chirped Delay Lines for Dispersion Compensation of 10-Gb/s Optical Communication Signals," *J. Lightw. Technol.*, vol.26, no.15, pp.2641-2646, Aug.1, 2008.
[20] F. Bolos, J. Blanco, A. Collado and A. Georgiadis, "RF Energy Harvesting from Multi-Tone and Digitally Modulated Signals," in *IEEE Transactions on Microwave Theory and Techniques*, vol. 64, no. 6, pp. 1918-1927, Jun. 2016.
[21] J. Bito, J. G. Hester and M. M. Tentzeris, "Ambient RF Energy Harvesting from a Two-Way Talk Radio for Flexible Wearable Wireless Sensor Devices Utilizing Inkjet Printing Technologies," in *IEEE Transactions on Microwave Theory and Techniques*, vol. 63, no. 12, pp. 4533-4543, Dec. 2015.
[22] S. Abbasian and T. Johnson, "High efficiency GaN HEMT synchronous rectifier with an octave bandwidth for wireless power applications," *2016 IEEE MTT-S International Microwave Symposium (IMS)*, San Francisco, CA, 2016, pp. 1-4.